Available online at www.sciencedirect.com
SCIENCE DIRECT®
International Journal of Mass Spectrometry 229 (2003) 27–34
International Journal of Mass Spectrometry
www.elsevier.com/locate/ijms

Nanoscopic surface modification by slow ion bombardment

I.C. Gebeshuber, S. Cernusca, F. Aumayr, H.P. Winter*

Institut für Allgemeine Physik, Technische Universität Wien, Wiedner Hauptstraße 8-10, A-1040 Vienna, Austria

Received 9 January 2003; accepted 24 January 2003

Abstract

We present systematic scanning tunneling microscopy (STM)/atomic-force microscopic (AFM) investigations on nanoscopic defect production at atomically clean surfaces of SiO_2, Al_2O_3 and highly oriented pyrolytic graphite (HOPG) after bombardment by slow (impact energy $\leq$ 1.2 keV) singly and multiply charged ions under strict ultra-high vacuum (UHV) conditions. Combined STM and AFM studies show that on HOPG only "electronic" but no visible topographic defects are created by such ion bombardment. On the monocrystalline insulator surfaces, well-defined topographic features of typically nm extensions are produced ("potential sputtering"). For Al_2O_3 and HOPG, a clear dependence of the defect size on the projectile ion charge is demonstrated. These results are discussed in view to possible new nanoscopic surface structuring and modification methods for which the kinetic projectile energy plays a minor role only.

Keywords: Ion–surface interaction; Potential sputtering; Surface defects; Multicharged ions

1. Introduction

Impact of slow ions on solid surfaces can give rise to inelastic processes which modify the geometric and electronic structure at and below the surface, cause emission of electrons and photons as well as neutral and ionized target particles (atoms, molecules, clusters), remove surface-adsorbed material and lead to projectile neutralization. The transfer of electrons between surface and projectile possibly acts as precursor for the above-mentioned processes and makes them to proceed irrespective of the kinetic projectile energy. The importance of such "electronic" processes increases with multicharged projectile ions and their role is elucidated when slow ions of same kinetic energy but with different charge states are applied as projectiles.

For certain insulator surfaces, the impact of slow multicharged ions (MCIs) Z^{q+} gives rise to considerably stronger ablation than the well-established kinetic sputtering by neutral or ionized projectiles. First experimental evidence for "potential sputtering" (PS) was reported for alkali-halide surfaces and explained by "Coulomb explosion" [1], i.e., creation of small positively charged surface spots from the rapid electron capture by impinging MCI, and the subsequent ablation because of strong mutual target ion repulsion. "Coulomb explosion" was also invoked in order to explain atomic-force microscopic (AFM) observations of blister-like defects on mica samples produced by highly charged ions Z^{q+} (kinetic energy 1–3 keV/amu) [2]. However, studies for impact of slow ($\leq$1 keV) MCI on thin polycrystalline films of alkali-halides (LiF, NaCl) and Al_2O_3 deposited on quartz microbalance crystals [3] suggested a different explanation for PS, namely defect-stimulated desorption induced by very efficient electron capture [4]. It has been established that such desorption processes are induced by electrons (ESD) or photons (PSD) on such materials where self-trapping of specific crystal defects proceeds via electron–phonon coupling in the crystal lattice [5]. However, such defect trapping as the prerequisite for PS may also be caused or at least supported by the kinetic projectile energy ("kinetically assisted PS" [6]), which could also explain some PS-like effects reported for target species where no electron–phonon coupling can take place, i.e., for semiconductors like Si and GaAs [2]. In any case, for slow ion impact the self-trapping mechanism is most relevant for PS. Consequently, for metal and semiconductor surfaces no slow MCI-induced PS can be observed, so far [7].

As the surface region from which a slow MCI does capture electrons should be rather small (nm extensions), it is

* Corresponding author. Tel.: +43-1-58801-13401; fax: +43-1-58801-13499.
E-mail address: winter@iap.tuwien.ac.at (H.P. Winter).

1387-3806/$ – see front matter © 2003 Elsevier Science B.V. All rights reserved.
doi:10.1016/S1387-3806(03)00252-5

probable that the surface defects caused by PS are of similar size. In order to study such defect structures we have applied AFM in ultra-high vacuum (UHV) on monocrystalline target surfaces of insulator species for which PS by slow MCI impact has already been demonstrated on polycrystalline thin films [3,6,7].

We have carried out AFM studies for, e.g., SiO_2 and Al_2O_3 (cf. Section 3) and obtained results which are of possible interest for nanostructuring these surfaces.

For comparison, similar studies have also been performed with a highly oriented pyrolytic graphite (HOPG) surface. As graphite is a good electrical conductor, no PS is expected to take place there. On the other hand, numerous studies have shown that for HOPG characteristic surface modifications can be produced by ion irradiation. In contrast to an insulator surface, for HOPG defects can be conveniently studied down to the atomic scale by means of scanning tunneling microscopy (STM), which has been applied with a combined AFM/STM setup (see Section 2). We could show (cf. Section 4) that impact of slow singly and multiply charged ions on a HOPG surface results in local modifications of the electronic structure but no topographical changes due to potential sputtering effects.

2. Experimental methods

Observations of slow ion-induced nanodefects on different atomically clean target surfaces have been made under strict UHV conditions with a combined AFM/STM instrument (UHV-AFM/STM, OMICRON Nanotechnology GmbH, Germany). We have looked for nanodefects on freshly prepared surfaces of SiO_2(0 0 0 1) and sapphire *c*-plane Al_2O_3(0 0 0 1) after irradiation with low doses of slow singly and multiply charged ions. In order to avoid disturbing noise from an ion irradiation chamber directly attached to the AFM/STM instrument, we have used a transportable UHV vault for target transfer which was alternatingly coupled via UHV locks to the target ion irradiation chamber and the AFM/STM. This procedure kept the target surfaces under permanent UHV conditions after initial cleaning, thermal annealing, and during subsequent slow ion irradiation until completion of the AFM/STM inspection. Ion irradiation of the insulator surfaces was accompanied by low-energy ($\leq$4 eV) electron flooding to compensate for surface charge-up which otherwise strongly inhibits AFM observation or makes it even impossible. The electron gun was arranged at 2 cm distance to the sample. All AFM observations were made in the contact mode, with the base pressure in the AFM/STM chamber kept at about 10^{-10} mbar during measurements.

HOPG is rather easy to prepare with surface terasses which extend over several hundreds of nm. The HOPG samples were cleaved in air with adhesive tape and immediately put into the ultra-high vacuum chamber (base pressure below 10^{-9} mbar). Before ion irradiation a sample was heated up to 300 °C, but during the irradiation experiment kept at room temperature. STM images were taken at constant current mode with negative sample bias voltage in the range of some mV to V and tunneling currents of 1–10 nA.

Electrochemically etched tungsten tips were used which provided excellent atomic resolution. Again, AFM data were taken in the contact mode.

The singly and multiply charged ions for target irradiation have been extracted from a 5 GHz ECR ion source [8], magnetically analyzed and guided via electrostatic lenses to the UHV irradiation chamber. The ions were decelerated in front of the target surface to their desired impact energy ($\leq$1.2 keV). Uniform irradiation was assured by rapidly scanning the ion beam across the target surface by means of deflection plates.

3. Production of slow ion-induced surface defects on insulator targets (Al_2O_3, SiO_2)

3.1. Al_2O_3

Polished Al_2O_3(0 0 0 1) *c*-plane single crystals (TBL Kelpin, Neuhausen, Germany) have been CO_2 snow cleaned and then annealed in UHV for 3 h at 400 °C. This preparation technique yields very flat crystal surfaces (see Fig. 1). AFM contact mode studies on 14 samples prepared by the standard preparation technique revealed a root mean square (rms) roughness of 0.093 ± 0.06 nm rms. Bombardment with Ar ions of different charge states and kinetic energies (500 eV Ar^+ and Ar^{7+}, 1.2 keV Ar^+, Ar^{4+} and Ar^{7+}) results—as seen in AFM contact mode—in hillock-like nanodefects (see Figs. 2 and 3).

We found that the ion-induced defects on the sapphire single crystal surface could be removed by annealing at 450 °C for 5 h. The density of nanodefects does not directly correspond with the applied ion dose: an ion dose of 5 ×

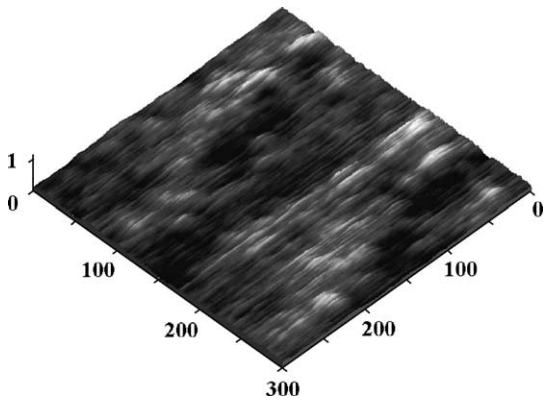

Fig. 1. UHV AFM contact mode image of a sapphire crystal prepared with standard single crystal preparation technique reveals very flat surfaces (rms *z* noise below 0.1 nm). Flat surfaces are a prerequisite for unambiguous assignment of the surface nanostructures produced by slow single ion impacts. All dimensions in nanometers.

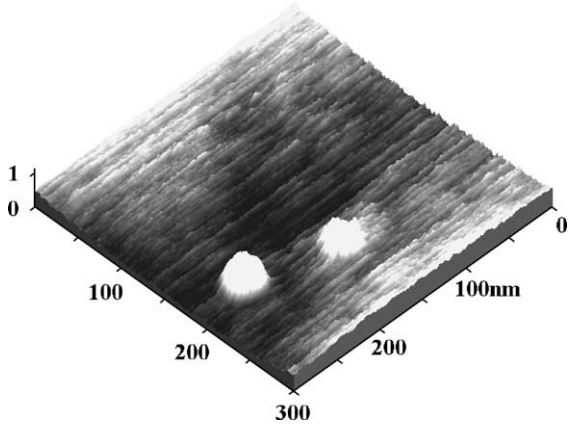

Fig. 2. UHV AFM contact mode image of sapphire (Al_2O_3, *c*-plane 0 0 0 1) bombarded with 500 eV Ar^+ ions. The defects are real topographic features; all dimensions in nanometers.

10^{12} ions/cm^2, which is equivalent to five ions per 10 nm × 10 nm, leads to a rather small, however reproducible, density of defects on the sapphire surface: about 10 nanodefects per 1000 nm × 1000 nm can be observed after bombardment in the energy range reported in this paper. This is equivalent to a dose to defect ratio of 5000. A possibly similar migration and subsequent recombination of point defects at the surface has previously been reported for silicon bombarded by 5 keV He ions above 160 K [9]. In fact, the only case where the number of defects corresponded fairly well to the applied ion dose was for the conducting HOPG samples (see Section 4).

The Al_2O_3 *c*-plane proved to be the insulator surface showing most clearly a dependence of the ion bombardment-induced defects with the kinetic energy and charge states of the projectiles. 500 eV Ar^+ ions produce defects which are about 1 nm high (Fig. 2) and have lateral dimensions of some tens of nanometers (one should keep in mind that the height is more accurately measurable with the AFM than lateral dimensions), whereas the defects produced by 500 eV Ar^{7+} ions are several nanometers high (Fig. 3) and show lateral dimensions of about 100 (!) nanometers. At higher kinetic energy the differences in the slow ion-induced nanodefects on the sapphire *c*-plane became even more distinct. 1.2 keV Ar^+-induced defects are up to about 8 nm high and their width is some 10 nm. For a higher charge state as Ar^{4+}, two different kinds of defects occurred on the sapphire surface. They have about the same height, but their lateral dimensions vary considerably: some are nearly 200 nm wide, whereas the smaller defects are only about 50 nm wide.

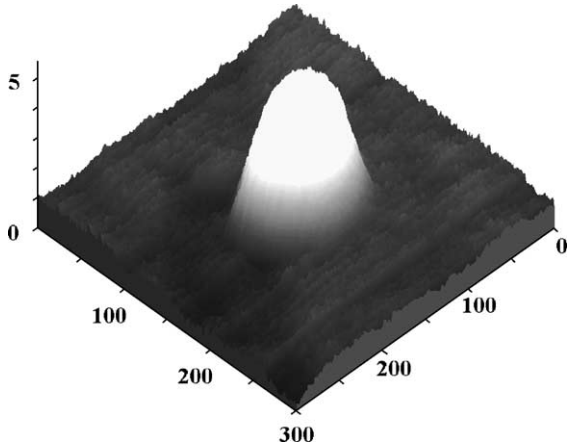

Fig. 3. UHV AFM contact mode image of sapphire (Al_2O_3, *c*-plane 0 0 0 1) bombarded with 500 eV Ar^{7+} ions. Nanodefects induced by these ions with same kinetic but higher potential energy as compared to Ar^+ ions (see Fig. 2) are considerably higher and wider than the ones caused by singly charged ions. All dimensions in nanometers.

The height of both kinds of defects is about 2 nm. For Ar^{7+}, only one kind of defect was visible in the AFM images, with about 50 nm diameter and about 2 nm height (for a more detailed description of these results, see Gebeshuber et al., 2003).

3.2. SiO_2

Polished SiO_2(0 0 0 1) α-quartz single crystals (TBL Kelpin, Neuhausen, Germany) were CO_2 snow cleaned and then annealed in UHV at 400 °C for 3 h. This preparation technique yielded very flat crystal surfaces. AFM contact mode studies on 14 such prepared crystals revealed a rms roughness of 0.16 ± 0.01 nm rms. The quartz crystals were then bombarded with 1 keV Ar^+ ions. UHV AFM imaging of the surface topography revealed ion-induced nanostructures, i.e., the surface was covered with hillocks a few nanometers high (see Fig. 4). The density of these hillocks did not directly correspond to the applied ion dose: for a dose of five incident 1 keV Ar^+ ions per 10 nm × 10 nm (5×10^{12} ions/cm^2), we observe about 30 nanostructures on an area of 1000 nm × 1000 nm, which indicates that not every single ion has caused one nanodefect on the quartz surface. The dose to defect ratio on the quartz substrate is about 1700. Probably several ion impacts are needed to induce one AFM-detectable surface modification. We could not yet establish an ion-charge state dependence of observed defects.

The fact that apparently hillocks are observed instead of craters is not yet understood. Several possible explanations can be given. In AFM as for other scanning probe microscopy (SPM) methods it is more straightforward to image elevated structures than craters. Narrow tall surface features in the vicinity of craters would completely mask the latter because of their convolution with the tip shape. Several other groups have used AFM as investigative method and reported hillock-like surface modifications after bombardment with heavy ions for up to GeV energies. By means of AFM, Audouard et al. [10] have studied the surface of amorphous metallic ribbons irradiated with swift heavy ions. Ion impacts resulted in the formation of hillocks at 300 K for ions with high stopping power of ≥55 keV/nm. However, irradiation at 80 K did not induce noticeable modifications of the surface of the ribbons. These results

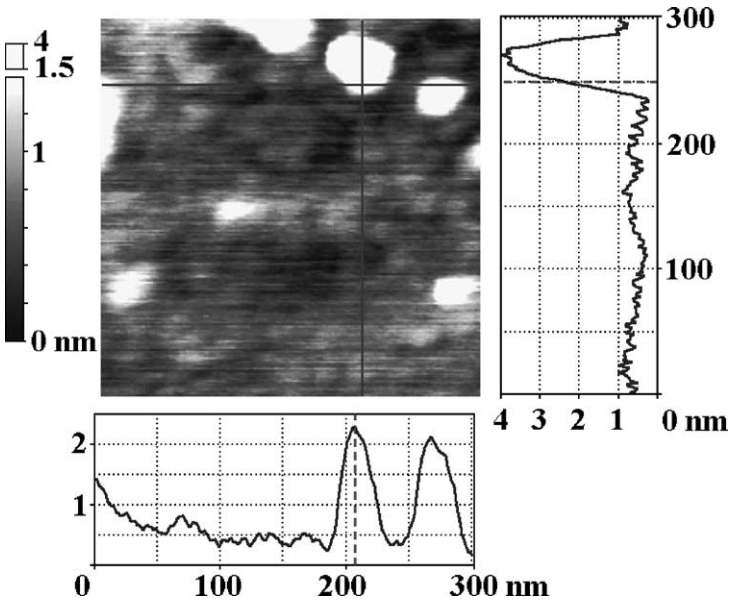

Fig. 4. Line profiles of SiO_2(0 0 0 1) single crystal surface after bombardment with 1 keV Ar^+ ions (UHV AFM contact mode).

indicate that formation of hillocks, which are flattened by the sample growth, is essentially caused by the damage created by electronic excitation in individual ion tracks. In another experiment, Audouard et al. [11] studied with AFM modifications of surface topography of amorphous metallic alloys irradiated with swift heavy ions. Irradiation with Pb or U ions with rather high stopping power $(dE/dx)_e$ led to the formation of hillocks surrounded by craters, whereas no visible modifications of the specimen surface was observed after irradiation with Kr ions with lower $(dE/dx)_e$. These authors ascribed formation of hillocks to the damage created in individual ion tracks, while craters were linked to anisotropic growth phenomena. Both processes are thus induced by severe electronic excitation in the wake of incident ions.

4. Slow ion-induced surface defects on HOPG

Surface defects in HOPG produced by the impact of individual (singly charged) ions have already been investigated via STM/AFM by a number of groups (see [12–21] and further references therein). However, only recently first results have been reported for impact of slow multiply charged ions and the effect of the projectile charge state (or potential energy) on the size of the produced nanodefects [22,23]. Moreover, in most previous studies either STM in air was used or the irradiated samples were transported in air towards STM inspection after ion bombardment. If, e.g., chemical bonds at the surface are broken due to the ion impact, impurities could preferentially adsorb at these

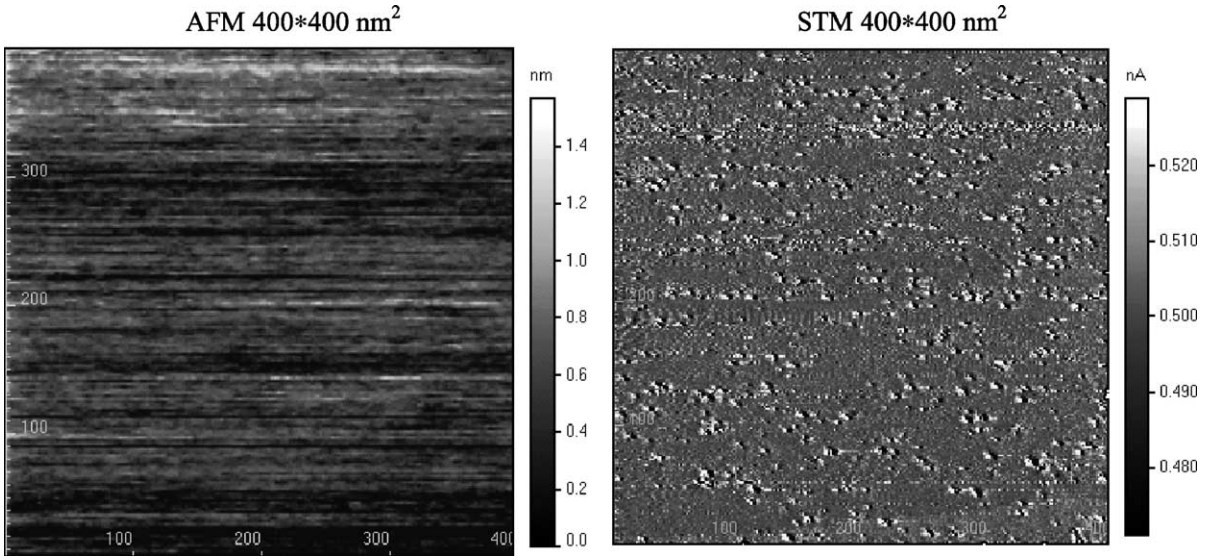

Fig. 5. AFM and STM scans of HOPG bombarded with 1200 eV Ar^+ ions. In the AFM scan no topographic changes can be detected. Only the STM reveals the defects in the electronic structure.

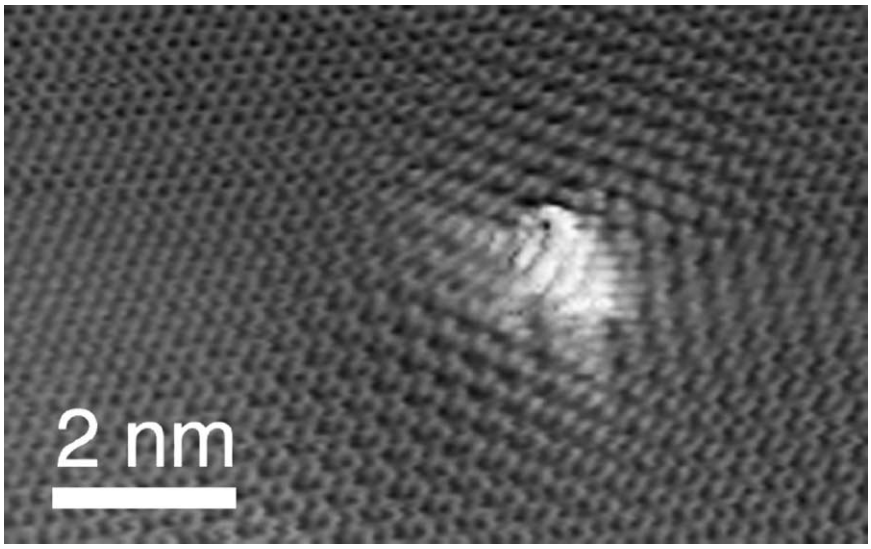

Fig. 6. STM image of defect produced by the impact of a single (150 eV) Ar^{9+} ion on HOPG.

sites and thus change the topography of the surface (and the resulting STM image) during contact with air. Therefore, in our studies MCI bombardment has been followed by STM/AFM investigations without breaking the ultra-high vacuum (see Section 2). In this way possible influences from target surface exposure to air could be ruled out.

Fig. 5 shows typical AFM and STM scans of HOPG samples bombarded with 1200 eV Ar^+ ions. In the AFM scan, no significant topographic changes can be detected. On the contrary, the STM image reveals a large number of individual nanosized defects as the result of the ion bombardment. Several hundred defects from different sample positions have been statistically analyzed for each projectile type (Ar^+, Ar^{8+}, Ar^{9+}). Fig. 6 shows the enlarged STM image of a typical defect on HOPG created by the impact of a single Ar^{9+} ion of 150 eV kinetic energy.

Figs. 7 and 8 show examples of STM 3D-images of a highly oriented pyrolitic graphite surface bombarded with 150 eV Ar^+ and Ar^{9+} ions, respectively. The images were taken from a 16-bit black and white graphics and processed by the SXM image program using a calculated shadow by illuminating the images from the right.

The only surface defects found in the STM images (cf. examples in Figs. 6–8) are "protrusions" (hillocks) with a mean lateral size of 0.8–1.25 nm and an average equivalent height of 0.22 nm. They are randomly dispersed on the originally flat surface. Their area density is in good agreement with the applied ion dose, implying that nearly every single ion impact has caused one protrusion. A $\sqrt{3} \times \sqrt{3}R30^\circ$ surface reconstruction, as characteristic for interstitial defects in HOPG [20,21,24], surrounded by undisturbed surface parts is observed in the vicinity of most defects (see Figs. 6–8).

Scanning with our AFM down to atomic resolution on the irradiated surface did not show any significant topological changes due to ion bombardment. Therefore, we conclude that the defects observed are mainly due to changes in the electronic density of states of the surface.

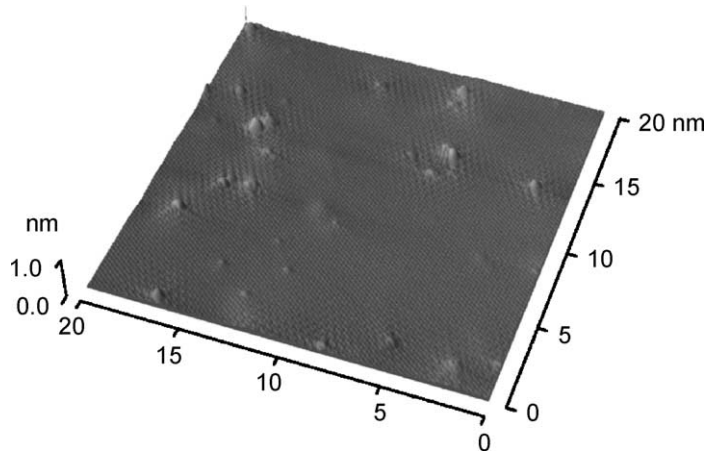

Fig. 7. STM image of HOPG surface bombarded by singly charged Ar ions of 150 eV kinetic energy (tunneling current: 0.58 nA, bias voltage: 0.5 V).

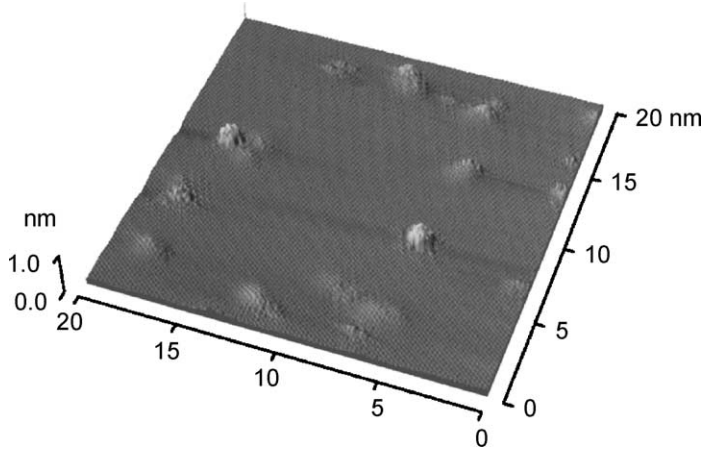

Fig. 8. STM image of HOPG surface bombarded by Ar^{9+} ions of 150 eV kinetic energy (tunneling current: 0.55 nA, bias voltage: 0.4 V).

For impact of singly charged ions, our findings are in good agreement with previous observations [16,21]. As a remarkable result, however, we find that the measured mean diameter of the "hillocks" and to a somewhat lesser extent their "height" increase with projectile charge state (see Fig. 9). The corresponding statistical distribution of the evaluated damage height and the full width at half maximum (FWHM) due to Ar^+ and Ar^{9+} ion bombardment of the HOPG surface are shown in Fig. 10.

In a careful STM study, Hahn and Kang [21] have shown that generally two kinds of defects in HOPG are created under low energy (100 eV) Ar^+ bombardment, namely carbon vacancy defects (VDs) and interstitial defects (IDs) formed by trapping the projectile beneath the first carbon plane. Both types of defects are detected as protrusions in the STM topographic image. The dangling bonds at the VD site cause an enhancement of the local charge density-of-states (CDOS) near the Fermi energy, seen as a protrusion in the STM image [21]. The protrusion observed in the STM image at ID sites results from a small geometric deformation of the graphite basal plane due to the trapped projectile (not large enough to be visible in our AFM scans) and an apparently larger electronic defect due to an increased CDOS. Only for IDs but not for VDs a $\sqrt{3} \times \sqrt{3}R30^\circ$ surface reconstruction was reported [21]. From this $\sqrt{3} \times \sqrt{3}R30^\circ$ superlattice structure also observed in our experiments (see Fig. 11), we, therefore, conclude that the majority of the "hillocks" observed are due to IDs, or VDs created along with IDs.

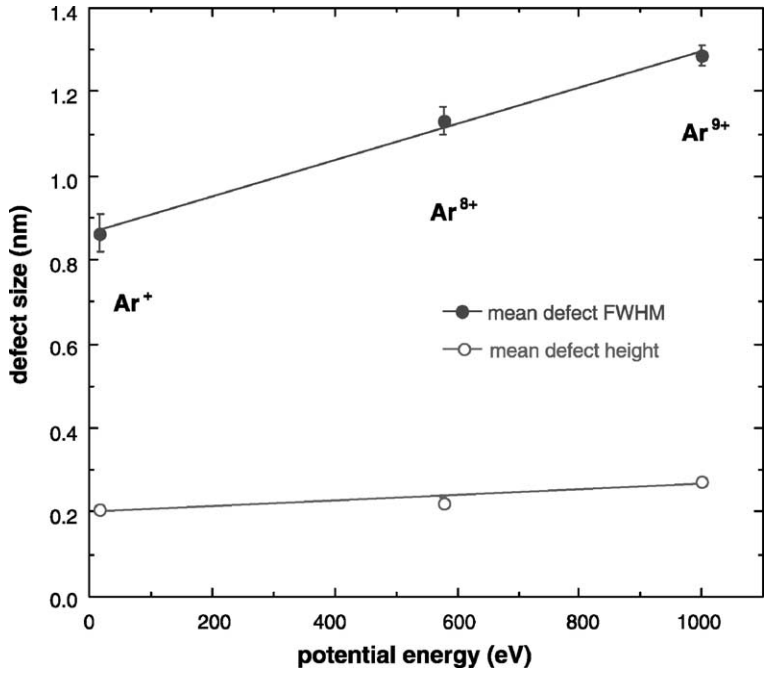

Fig. 9. Mean height and width (FWHM) of defect structures produced by impact of 150 eV Ar^{q+} (q = 1, 8, 9) ions on HOPG. For each projectile species data were obtained from different STM images by evaluating all visible defects.

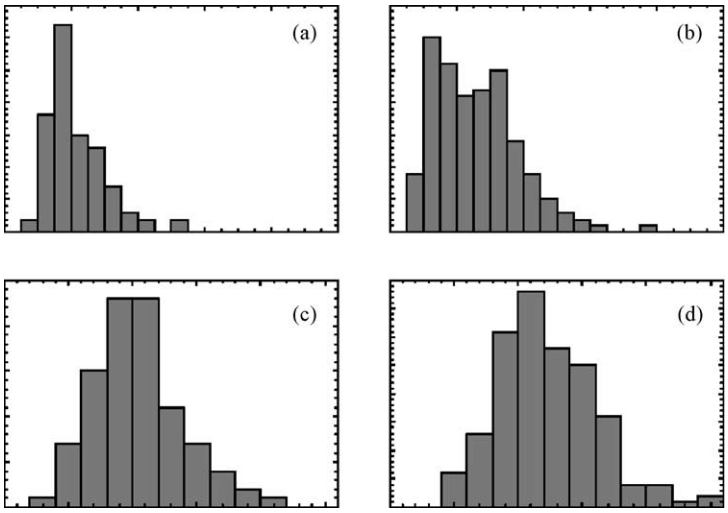

Fig. 10. Statistical distribution of damage height (a, b) and full width at half maximum (FWHM) (c, d) due to singly charged Ar ion impact (a, c) and Ar^{9+} ion impact (b, d) on HOPG.

The strong increase of the lateral protrusion size with increasing charge state of the projectile ion is interpreted as a "pre-equilibrium" effect of the stopping of slow multiply charged ions in HOPG, as has so far only been observed for higher charge states [17]. Although MCI are converted already into neutral hollow atoms during their approach towards the surface, their captured electrons remain in highly exited states until surface impact, where they are gradually

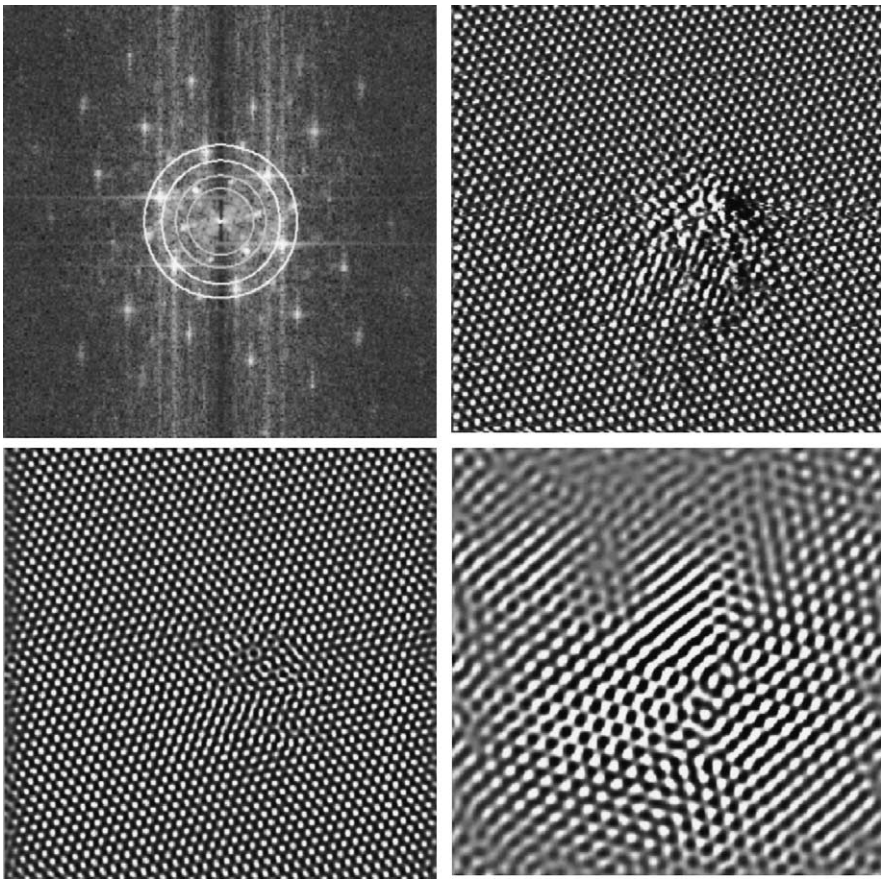

Fig. 11. Fourier transform (top left) of a tunneling current image of a Ar^{+} ion-induced defect on HOPG (top right). Filtering and inverse fast Fourier transformation allow for separation of the contributions from the undisturbed crystal lattice (bottom left, reconstructed from frequencies within the white circles) and ion-induced superstructure (bottom right, reconstructed from frequencies within the green circles), respectively. Top left and bottom tunneling current images 10 nm × 10 nm.

peeled off and replaced by conduction band electrons forming a partial screening cloud around the MCI [25]. Before final deexcitation of the hollow atom can take place within the solid, reduced screening should result in a strongly increased energy loss of the projectiles. According to SRIM 2000 calculations [26], the mean range of 150 eV Ar projectiles in HOPG is about two monolayers. An increased stopping and straggling of the higher charged Ar projectiles would lead to IDs located closer to the surface, as well as to more VDs due to a higher momentum transfer to the carbon atoms of the first plane. Because of the extreme surface sensitivity of STM this pre-equilibrium effect in the stopping power is not masked by (equilibrium) bulk effects and apparently observable with unprecedented clearness. From this AFM data we conclude that the nanodefects produced by slow ion impact are of electronic rather than of topographic nature.

5. Summary and conclusions

In this paper, we have described first evidence for potential sputtering (PS) effects on some atomically clean monocrystalline insulator surfaces, which was obtained by means of UHV AFM. Target samples were bombarded with slow (typically <1 keV) singly and multiply charged Ar^{q+} ions (up to $q = 7$). Keeping these target surfaces permanently under UHV conditions during initial annealing, ion irradiation and AFM inspection was found indispensable for obtaining unambiguous evidence for PS, i.e., nanodefects with a size clearly depending on the slow ion charge state. The fact that the observed number of defects does not correspond one-to-one to the ion dose will be investigated in more detailed experiments with different ion doses. Analysis of the statistics of random impacts will clarify how many individual ion impacts are needed to form a visible nanodefect on the insulator surface. In particular, Al_2O_3 was identified as a good candidate for PS-induced nanostructuring, and further studies for SiO_2 might probably lead to similar results. Both target materials are relevant for applications in microelectronics and nanotechnology.

In addition, we have searched for slow ion-induced nanodefects on atomically clean HOPG. Extending pertinent work by other groups with singly charged ions only, our combined STM/AFM studies revealed nanodefects which comprise a disturbance of the electronic density-of-states of the surface rather than its topography. Whereas the size of these defects increases with the ion charge (here up to $q = 9$), as expected for any conducting target surface they showed no evidence for potential sputtering.

Acknowledgements

This work has been supported by Austrian FWF under project no. 13543-PHY. The authors thank Dr. R. Wörgötter-Plunger for her cooperation in the early studies of insulator surfaces. Initial work with HOPG has greatly benefited from support by Drs. M. Schmid and P. Varga.

References

[1] I.S. Bitensky, M.N. Murakhmetov, E.S. Parilis, Sov. Phys. Tech. Phys. 25 (1979) 618.
[2] D.H. Schneider, M.A. Briere, J. McDonald, J. Biersack, Radiat. Eff. Defects Solids 127 (1993) 113;
T. Schenkel, A.V. Hamza, A.V. Barnes, D.H. Schneider, Progr. Surf. Sci. 61 (1999) 23.
[3] G. Hayderer, M. Schmid, P. Varga, H.P. Winter, F. Aumayr, Rev. Sci. Instrum. 70 (1999) 3696.
[4] F. Aumayr, J. Burgdörfer, P. Varga, H.P. Winter, Comments At. Mol. Phys. 34 (1999) 201.
[5] P. Townsend, in: R. Behrisch (Ed.), Sputtering by Particle Bombardment II, Springer, Berlin, 1983, Chapter 4, p. 147.
[6] G. Hayderer, S. Cernusca, M. Schmid, P. Varga, H.P. Winter, F. Aumayr, D. Niemann, V. Hoffmann, N. Stolterfoht, C. Lemell, et al., Phys. Rev. Lett. 86 (2001) 3530.
[7] P. Varga, T. Neidhard, M. Sporn, G. Libiseller, M. Schmid, F. Aumayr, H.P. Winter, Phys. Scr. T73 (1997) 307.
[8] M. Leitner, D. Wutte, J. Brandstötter, F. Aumayr, H.P. Winter, Rev. Sci. Instrum. 65 (1994) 1091.
[9] P.J. Bedrossian, T.D. de la Rubia, J. Vac. Sci. Technol. A 16 (1998) 1043.
[10] A. Audouard, R. Mamy, M. Toulemonde, G. Szenes, L. Thome, Nucl. Inst. Meth. Phys. Res. B 146 (1998) 217.
[11] A. Audouard, R. Mamy, M. Toulemonde, G. Szenes, L. Thome, Europhys. Lett. 40 (1997) 527.
[12] L. Porte, C.H. de Villeneuve, M. Phaner, J. Vac. Sci. Technol. B 9 (1991) 1064.
[13] R. Coregater, A. Claverie, A. Chahboun, V. Landry, F. Ajustron, J. Beauvillain, Surf. Sci. 262 (1992) 208.
[14] H.X. You, N.M.D. Brown, K.F. Al-Assadi, Surf. Sci. 279 (1992) 189.
[15] T. Mazukawa, et al., Appl. Surf. Sci. 107 (1996) 227.
[16] K. Mochiji, S. Yamamoto, H. Shimizu, S. Ohtani, T. Seguchi, N. Kobayashi, J. Appl. Phys. 82 (1997) 6037.
[17] K.P. Reimann, W. Bolse, U. Geyer, K.P. Lieb, Europhys. Lett. 30 (1995) 463.
[18] S. Habenicht, W. Bolse, H. Feldermann, U. Geyer, H. Hofsäss, K.P. Lieb, F. Roccaforte, Europhys. Lett. 50 (2000) 209.
[19] R. Neumann, et al., Nucl. Instrum. Meth. B 151 (1999) 42.
[20] R. Hahn, K. Kang, S. Song, J. Jeon, Phys. Rev. B 53 (1996) 1725.
[21] R. Hahn, K. Kang, Phys. Rev. B 60 (1999) 6007.
[22] R. Minniti, L.P. Ratliff, J.D. Gillaspy, Phys. Scr. T92 (2001) 22.
[23] G. Hayderer, S. Cernusca, M. Schmid, P. Varga, H.P. Winter, F. Aumayr, Phys. Scr. T92 (2001) 156.
[24] A.V. Krasheninnikov, F. Elsin, Surf. Sci. 454–456 (2000) 519.
[25] H.P. Winter, F. Aumayr, J. Phys. B: At. Mol. Opt. Phys. 32 (1999) R39;
A. Arnau, Surf. Sci. Rep. 229 (1997) 1.
[26] J.F. Ziegler, J.P. Biersack, U. Littmark, The Stopping and Range of Ions in Matter, vol. 1, Pergamon, New York, 1985.